First-principles study of luminescence properties of the Eu-doped defect pyrochlore oxide $KNbWO_6 \cdot H_2O$:0.125Eu^{3+}

Song-Hyok Choe,[1,*] Chol-Jun Yu,[1,†] Myong Choe,[1] Yun-Hyok Kye,[1] Yong-Nam Han,[2] and Guangsheng Pang[3]

[1]*Chair of Computational Materials Design, Faculty of Materials Science, Kim Il Sung University, Ryongnam-Dong, Taesong District, Pyongyang, Democratic People's Republic of Korea*

[2]*Faculty of Chemistry, Kim Il Sung University, Ryongnam-Dong, Taesong District, Pyongyang, Democratic People's Republic of Korea*

[3]*State Key Laboratory of Inorganic Synthesis and Preparative Chemistry, College of Chemistry, Jilin University, Changchun 130012, People's Republic of China*

(Received 26 February 2020; accepted 30 June 2020; published 20 July 2020)

Defect pyrochlore oxides have attracted great interest as a promising luminescent material due to their flexible composition and high electron/hole mobility. In this paper, we investigate the structural and electronic properties of lanthanide-doped (Ln) defect pyrochlore oxides $KNbWO_6$:0.125Ln^{3+} by using first-principles calculations. We perform structural optimizations of various defect pyrochlore models and calculate their electronic structures, revealing that hydration has a significant influence on both the local symmetry around the Eu^{3+} ion and the band structure with an alteration of their luminescent behavior. In the hydrated compounds, the electric-dipole $^5D_0$-$^7F_2$ transition is found to be partially suppressed by a raised local symmetry, and the water molecules in the compounds can mediate the nonradiative energy transfer between the activator Eu^{3+} ions and the host. It turns out that the oxygen vacancies are detrimental to luminescence as they reduce the Eu^{3+} ion in its vicinity to the Eu^{2+} ion and also serve as traps for conduction electrons excited by incident light. Our calculations for $KNbWO_6$:0.125Ln^{3+} (Ln=Ce, Pr, Nd, Pm, Sm) support that the defect pyrochlore oxide $KNbWO_6$ can also be used as a luminescence host for Ln^{3+} ion doping, giving valuable insight into a variation trend in luminescent properties of these materials at the atomic level.

DOI: 10.1103/PhysRevB.102.035131

I. INTRODUCTION

During the past half century, lots of luminescent materials have been discovered with various applications in many areas, including fluorescent lamps [1], photovoltaics and photocatalysts [2–4], bioimaging [5], and white light applications [6]. In order to improve the efficiency, lifetime, and environmental friendliness, much effort has been devoted to develop advanced luminescent materials containing the lanthanide (Ln) ion dopant, such as oxides ZrO_2:Tm^{3+}, Tb^{3+}, Eu^{3+} [7], silicate nitrides $LaSi_3N_5$:Ce^{3+} [8], and phosphates $LaPO_4$:Eu^{3+} [9]. Among many other inorganic compounds used for luminescence hosts, hollow crystal structures were known to be desirable for accommodating the Ln ions with large ionic radii. In this sense, several pyrochlore compounds with a large channel structure were expected to be a promising luminescent host [10–12].

Some years ago, we synthesized the hydrated defect pyrochlore oxide $KNbWO_6 \cdot H_2O$ and identified the luminescence properties by experimental measurements [13,14]. Furthermore, we prepared the Eu-doped hydrated defect pyrochlore $KNbWO_6 \cdot H_2O$:xEu^{3+} by applying an ion exchange under a hydrothermal condition [13]. In general, the Eu^{3+} ions were known to exhibit a characteristic red emission and to be excited by ultraviolet (UV) light. They are noticeable for symmetry-sensitive emission because of a nondegenerate ground state $^7F_0$ and nonoverlapping $^{2s+1}L_J$ multiplets [15]. In the case of $KNbWO_6 \cdot H_2O$:xEu^{3+}, emission spectra with strong peaks at 580, 594, and 612 nm were observed, together with excitation spectra with peaks at 394 and 464 nm. All these peaks in the emission/excitation spectra were identified as corresponding to intraconfigurational f-f transitions of $4f$ electrons of the Eu^{3+} ion. The emission intensity was found to be the strongest at a Eu-doping concentration of $x = 0.131$, and to get much stronger after it was annealed at 450 °C for 2 h. After annealing, the lifetime of the emission also became significantly longer due to the effect of dehydration during annealing, implying that hydration might be a possible reason for luminescence quenching. The dehydration of $KNbWO_6 \cdot H_2O$:xEu^{3+} was also found to influence the local symmetry of the Eu^{3+} ion, evidenced from the fact that the intensity of the emission peak at 612 nm, originating from the electric-dipole $^5D_0$-$^7F_2$ transition, was strengthened as much as ten times after annealing, while the magnetic-dipole $^5D_0$-$^7F_1$ transition spectra at 594 nm got slightly stronger. These results indicate that $KNbWO_6 \cdot H_2O$ can be used as an efficient luminescent host. In spite of such experimental findings, theoretical or computational studies on this material have yet to be performed, and thus there is a lack of atomistic insight into its luminescent properties.

The Ln-doped luminescence materials have been the subject of many first-principles studies within the density-functional theory (DFT) framework. In DFT calculations of Ln-doped materials, where the luminescence properties are

*sh.choi0220@ryongnamsan.edu.kp
†cj.yu@ryongnamsan.edu.kp

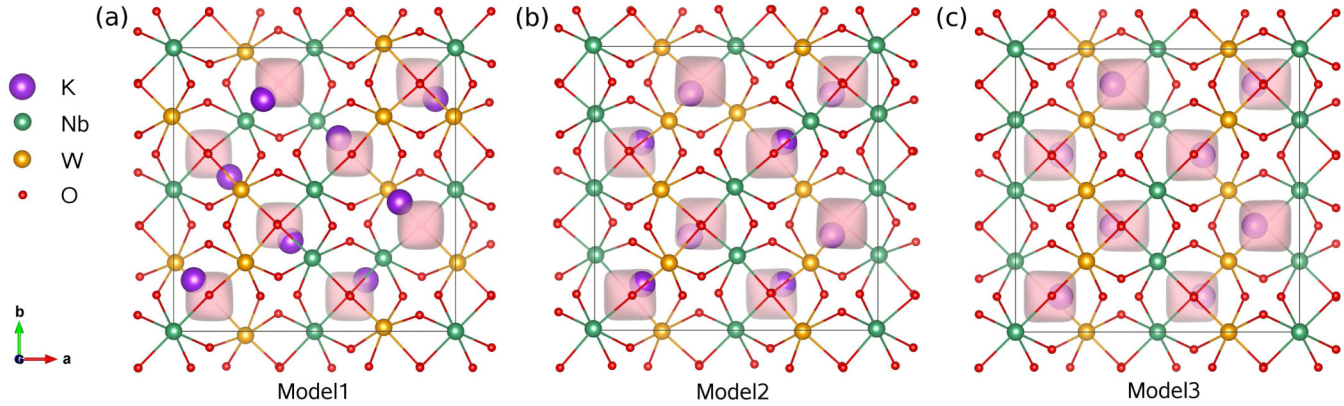

FIG. 1. Ball-and-stick top view of unit cells, optimized by using the PBEsol+U method, for the defect pyrochlore oxide $KNbWO_6$ in three different models, distinguished by the distribution of Nb/W atoms: (a) disorder (model 1), (b) semidisorder (model 2), and (c) order (model 3) models. Tetrahedronlike polyhedra in the light pink color indicate the BVS isosurface at a value of 1 for the K atom.

governed by transitions between the multielectronic states of the activator Ln ions involving $4f$ electrons, the challenge is to consider the $4f$ electrons explicitly. What is worse, as a single-particle ground-state theory, DFT cannot directly explain the transitions between the multielectronic states. In fact, many DFT studies have focused on $4f$-$5d$ transitions mainly occurring in Ce^{3+} and Eu^{2+} ions by employing the constrained DFT method to estimate the transition energy and Stokes shift [8,16,17], and to give an explanation about some luminescence properties such as the thermal quenching effect [18]. However, it was found to be almost impossible for DFT calculations to reproduce the experimentally observed spectra, which were formed by intraconfigurational $4f$-$4f$ transitions. Nevertheless, DFT calculations have been generally accepted to provide sufficiently reliable information on the crystalline structure and activator-ligand interaction in Ln-doped materials, which is important for estimating the trend in luminescence properties. Moreover, the DFT electronic structures can be used to determine the positions of the activator levels relative to the host band edges, which are also important for finding optical host-activator combinations [19]. The effect of defects in the host compound on the luminescence property can also be investigated with DFT calculations [20,21].

In this paper, we perform DFT calculations on several models related to the Eu-doped hydrated pyrochlore oxide $KNbWO_6 \cdot H_2O$:xEu to investigate the effect of hydration and defects on its luminescence property at the atomic level. The optimized structures of various defect-containing models are determined by structural relaxations and subsequently their electronic structures are calculated, determining the position of the $4f$ levels relative to the host band edges. We discuss the potential use of these compounds as a luminescence host for doping other trivalent Ln ions. In the remaining part of this paper, computational methods are given in Sec. II, the results and discussion in Sec. III, and the main conclusions in Sec. IV.

II. METHODS

A. Structural models

Defect pyrochlore oxides with a chemical formula AB_2O_6 are known to crystallize in a cubic phase with a space group of $Fd\bar{3}m$. The crystalline lattices are composed of corner-sharing BO_6 octahedra network with three-dimensional (3D) large channels, inside which the A cations are located, and the conventional unit cell contains 8 formula units (72 atoms). In the case of $KNbWO_6$, the B sites are randomly occupied by Nb and W cations at the same probabilities, while K cations randomly occupy one of every four equivalent crystallographic A sites. In order to visualize the plausible locations for the K cation, we carried out a bond valence sum (BVS) analysis in a relatively complex three-dimensionally linked structural framework [22,23] [see Fig. S1(a) for the isosurface plot at BVS = 1 for the K cation in the Supplemental Material [24]]. From the BVS analysis, it became clear that in the unit cell there are eight separate closed hollow spaces, resembling a tetrahedron, inside which one K^+ cation locates on any one of four vertex points as depicted in Fig. 1. Meanwhile, the configuration of Nb and W cations on the B sites is truly random, and thus three different models were suggested in this work. As illustrated in Fig. 1, model 1 represents the rather random distribution of Nb and W atoms along both the [100] and [010] directions, while models 2 and 3 show the alternating arrangement of Nb and W atom rows with one exception of the Nb/W atom exchange and without exception along the [100] direction. We could therefore distinguish these models by Nb and W atoms ordering along the [100] direction: model 1 for disorder, model 2 for semidisorder, and model 3 for order.

When hydrating the pyrochlore oxide, the resultant $KNbWO_6$:H_2O does not change the original crystalline lattice symmetry as the cubic phase with a space group of $Fd\bar{3}m$, with a lattice constant of $a = 10.5073$ Å and 8 formula units (96 atoms) in the unit cell [25]. In this hydrated pyrochlore structure, the water molecules reside inside the hollow spaces and thus the K^+ cations are pushed out from the hollow spaces [see Fig. S1(b) in the Supplemental Material [24]]. With a random placement of a water molecule on any one of the four equivalent hollow positions, we also suggested three different models for the $KNbWO_6$:H_2O crystal structure, distinguished by the configuration of the Nb/W atom distribution on the B sites. Meanwhile, for doping structures with Eu ions, three K^+ ions should be replaced by one Eu^{3+} ion on the A sites to satisfy the electronic charge neutrality, leading to the formation of one doped Eu^{3+} ion and two potassium vacancies

V_K. As these vacancies can appear in any two of the eight K sites in the unit cell except for the Eu-K substitution one, we again suggested three different Eu-doped models for each Nb/W configuration model and determined the lowest-energy configuration for the Eu-K substitution and V_K sites. Due to the sufficiently large size of the lattice constants exceeding 10 Å and the number of atoms being over 80, we can safely use the unit cell in the investigation of a doped material rather than using the supercell. Based on the experiment with a small amount of Eu atoms, only one Eu atom was supposed to be exchanged in the unit cell, leading to the compounds with a chemical formula of $KNbWO_6$:$0.125Eu^{3+}$ for nonhydrated pyrochlore oxide and $KNbWO_6 \cdot H_2O$:$0.125Eu^{3+}$ for the hydrated one, respectively.

B. Computational details

All the calculations in this work were carried out by means of the pseudopotential plane-wave method within the DFT framework, as implemented in QUANTUM ESPRESSO (QE) package (version 6.2) [26]. As being available from the GBRV Library [27], ultrasoft pseudopotentials (USPPs) were used to describe the ion-electron interaction. In the structural optimization, the exchange-correlation interaction between the valence electrons was considered by using the Perdew-Burke-Ernzerhof (PBE) functional [28] and its revised version for solids (PBEsol) [29] within the generalized gradient approximation (GGA). In addition, the Hubbard U term was taken into account for the d states of Nb, W, and Eu atoms. The Hubbard U parameter is in general fitted to available experimental data such as the band gap. Here, we tried to determine the U parameter so as to give the experimental band gap of $KNbWO_6$ (3.5 eV); the U value of 3 eV for Nb/W yielded a band gap of 3.0 eV. When increasing the U value for Nb/W from 3 to 6 eV, the band gap was found to increase only ∼0.1 eV, i.e., from 3.0 to 3.1 eV, indicating that larger U values have a negligible impact on the band gap. Recently, Timrov *et al.* [30] proposed an efficient approach to calculate the Hubbard parameters from density-functional perturbation theory (DFPT). Owing to the relatively large unit cell with more than 70 atoms, however, the DFPT approach is still computationally very expensive for our calculation. Therefore, we employed the U parameters of 3 eV for the Nb/W $4d/5d$ state and 4.0 eV for the Eu $5d$ state as already used in a previous work [8]. The kinetic energy cutoff for the plane-wave basis sets was set to be 60 and 500 Ry for the wave function and electron density, respectively. The Monkhorst-Pack [31] special k points for the Brillouin zone integration were set to be (2×2×2) for the structural optimization. These computational parameters guarantee a total energy accuracy of 5 meV per formula unit. The positions of all atoms and lattice constants were fully relaxed until the atomic forces converged to 0.02 eV/Å. Once the optimized structure for each $KNbWO_6$-derived compound was found, the host lattice constants were kept fixed while allowing the relaxation of atomic positions in the defect calculations.

In the electronic structure calculations including the energy bands and density of states (DOS), we only used the PBEsol functional, since it could give a better result than PBE when compared with the experimental lattice constants. Spin polarization was considered and *the* denser k points of (4×4×4) were used. For the doped models, the $4f$ electrons of Eu were explicitly treated as the valence electrons by using USPP from the PS LIBRARY (version 1.04) [32], where the valence electron configuration is $5s^2 6s^2 5p^6 4d^{10} 5d^{0.5} 4f^{6.5}$. In such $4f$ state-explicit calculations, larger cutoff energies of 90 and 800 Ry were used for a safe convergence and $U = 7$ eV was used for the strongly correlated $4f$ electrons of Eu [8]. The other doped models with Ln ions (Ce, Pr, Nd, Pm, Sm) were also investigated by using the same computational parameters for the case of Eu doping, except for the U parameters in the f-explicit calculations set differently as 4 eV for Ce [21], 5 eV for Pr/Nd, and 6 eV for Pm/Sm.

TABLE I. Lattice constant (a, b, c), average K-O interatomic distance ($d_{K\text{-}O}$), unit cell volume, and total energy difference per atom (ΔE) in three different $KNbWO_6$ models shown in Fig. 1, calculated with PBE and PBEsol XC functionals.

Model	Lattice constant (Å) a	b	c	$d_{K\text{-}O}$ (Å)	Volume (Å^3)	ΔE (meV)
		PBE				
Model 1	10.44	10.51	10.44	3.25	1147.50	0.00
Model 2	10.43	10.43	10.47	3.40	1139.72	0.09
Model 3	10.51	10.40	10.40	3.47	1137.62	5.21
		PBEsol				
Model 1	10.37	10.41	10.37	2.91	1120.46	0.00
Model 2	10.35	10.35	10.38	2.99	1113.92	2.22
Model 3	10.38	10.32	10.32	3.23	1107.61	7.03
Expt. [33]	$a = b = c = 10.36$				1112.84	

III. RESULTS AND DISCUSSION

A. Structural property

First, we carried out a structural optimization of the unit cells for the three different $KNbWO_6$ models by using the PBE and PBEsol exchange-correlation (XC) functionals. By comparing with the experimental lattice constants, the result can be used as a check on the validity of the computational parameters and XC functionals. Table I presents the obtained lattice constants and volumes of the unit cells for the three different models in comparison with the experimental data. We note that when allowing a full relaxation of the lattice parameters and atomic positions, the optimized crystal structures deviated from the cubic system as obtaining different lattice constants of $a \neq b$ or $a \neq c$ or $b \neq c$, which can be thought to be caused by a somewhat artificial (random) distribution of the atoms. In this situation, the unit cell volume was also provided to make it easy to do a comparison with experiment. It turned out that when compared with the experiment, the PBE functional yielded an overestimation of lattice constants with relative errors of 3.1%, 2.4%, and 2.2% for model 1, model 2, and model 3, whereas the PBEsol functional provided a good estimation of lattice constants with lower relative errors of 0.7%, 0.1%, and 0.5%, respectively. This indicates that the PBEsol functional is more adequate for defect pyrochlore oxides than the PBE functional and the

computational parameters used in this work are sufficiently reliable to give their accurate material properties. Therefore, only the PBEsol functional will be used in the following calculations.

In order to pick out the most stable model among the three different models, we present their total energy differences with respect to the lowest one in Table I. Model 1, the disorder model for Nb/W distribution on the B sites, was found to have the lowest total energy, while the order model 3 for Nb/W sublattices had the highest total energy with total energy differences of 5.21 and 7.03 meV/atom in the PBE and PBEsol calculations, respectively. It is worth noting that such a tendency in total energy is very consistent with the disorder degree of Nb/W distribution on the B sites and can be associated with the strength of the interaction between the K^+ cations and the oxygen anions. In order to compare the K-O interaction strength between the different models, we estimated the average of interatomic distances between K and its nearest six O atoms for each K atom, and then again the average over eight K-O distances in the unit cell. The estimated average K-O distance $d_{K\text{-}O}$ for each model is also given in Table I. We can see that $d_{K\text{-}O}$ becomes longer going from model 1 to model 2 and to model 3, suggesting a weakening of the K-O interaction. In fact, as shown in Fig. 1 for the optimized atomistic structures of the unit cells for the three different models, the K^+ cations reside at the edge of the BVS tetrahedron in model 1, formed by an isosurface value of BVS = 1 that displays the hollow spaces for the K^+ cations, while in model 3 they are located a little inside the BVS tetrahedron, farther from the neighboring O atoms.

Using the PBEsol functional, we then carried out the structural optimization of the unit cells for the hydrated pyrochlore $KNbWO_6 \cdot H_2O$ with three different models (models 1, 2, and 3) and for the Eu-doped pyrochlore $KNbWO_6$:0.125Eu^{3+} with nine different models (models 1-1, 1-2, 1-3, 2-1, . . ., 3-3) due to the three different configurations for Eu-K substitution and accompanying two V_K sites for each Nb/W configuration model. The obtained lattice constants and total energy differences of all the unit cells are presented in Table S1 [24]. Unlike the original pyrochlore oxide, the lowest-energy models were found to be based on model 2 (semidisorder model) for the hydrated and doped pyrochlore oxide. For the Eu-doped hydrated pyrochlore $KNbWO_6 \cdot H_2O$:0.125Eu^{3+}, therefore, we constructed two different unit cells of the Eu exchange based on the optimized model 2 of $KNbWO_6 \cdot H_2O$ due to whether the water molecules are aggregated around Eu^{3+} ion or evenly distributed (see Table S1 in the Supplemental Material [24]). In Table II, we summarize the optimized lattice constants and unit cell volumes of the energetically most favorable models for the original, hydrated, doped, and hydrated-doped pyrochlore compounds, obtained by using the PBEsol functional, in comparison with the available experimental data for the unit cell volume. For the sake of brevity, the original $KNbWO_6$ is termed as Orig, the hydrated $KNbWO_6 \cdot H_2O$ as Hyd, the Eu-doped $KNbWO_6$:0.125Eu^{3+} as Dop, and the hydrated Eu-doped $KNbWO_6 \cdot H_2O$:0.125Eu^{3+} as HydDop in the following. The optimized unit cell volumes can be said to be in good agreement with the experimental values as their relative errors of 0.68% in Orig, 0.92% in Hyd, and 0.50% in HydDop models, again indicating the reliance of our models and computational method. It was found that the volume expanded with hydration while it shrank with Eu doping.

TABLE II. Lattice constants (a, b, c) and unit cell volume of the most stable models for $KNbWO_6$ (denoted as Orig), $KNbWO_6 \cdot H_2O$ (Hyd), $KNbWO_6$:0.125Eu^{3+} (Dop), and $KNbWO_6 \cdot H_2O$:0.125Eu^{3+} (HydDop), calculated with the PBEsol functional and U method.

	Lattice constants (Å)			Volume (Å^3)	
Model	a	b	c	Calc.	Expt.
Orig	10.37	10.41	10.37	1120.46	1112.84 [33]
Hyd	10.50	10.52	10.39	1149.32	1160.04 [25]
Dop	10.38	10.33	10.36	1111.31	
HydDop	10.45	10.50	10.39	1138.72	1144.44 [13]

Figure 2 shows the crystalline structures of the Hyd, Dop, and HydDop models. When hydrating the original pyrochlore oxide $KNbWO_6$, the water molecules were found to penetrate into the hollow spaces where the K^+ cations already reside, resulting in a volume expansion, as shown in Fig. 2(a). One can see that the water molecules are located on the inner side of the hollow spaces and thus the K^+ cations move to the outer side when compared with nonhydrated pyrochlore, getting closer to the neighboring oxygen atoms. On the other hand, the K^+ cations in the Dop model maintain their locations as in the Orig model, while the inserted Eu^{3+} ion is clearly away from the BVS tetrahedron, as shown in Figs. 2(b) and 2(c). In fact, due to its higher valence, the Eu^{3+} cation tends to interact more strongly with the neighboring O^{2-} anions than the K^+ cation, so that it resides in the middle position between the hollow spaces. It should be noted that such a strengthening of the Eu-O binding leads to the contraction of volume when doping Eu into the defect pyrochlore oxide. For the case of the HydDop model shown in Fig. 2(c), the location of the Eu^{3+} cation was found to be similar to the case of the Dop model and the K^+ cations to be located in a position similar to the case of the Hyd model.

We further consider the local symmetry of the Eu^{3+} ion in the hosts, which plays a critical role in luminescence as it determines the emission wavelength and intensity due to the intraconfigurational $4f$-$4f$ transition [34,35]. It is well known that for the case of the Eu^{3+} ion being at an inversion symmetry site, the electric-dipole $^5D_0$-$^7F_2$ transition is parity forbidden, while the magnetic-dipole $^5D_0$-$^7F_1$ transition is parity allowed with a dominant emission wavelength around 590 nm. Meanwhile, at a noninversion symmetry site, the Eu^{3+} ion was known to exhibit an electric-dipole $^5D_0$-$^7F_2$ transition with an emission wavelength of 610–620 nm, whose intensity is hypersensitive to the site symmetry of Eu^{3+} [11]. In several Eu-doped pyrochlore oxides with luminescence, both the electric- and magnetic-dipole transitions appear simultaneously, one of which is much stronger in most cases [11,12,34,35]. In the case of the defect pyrochlore oxide $KNbWO_6$, the location of doped Eu^{3+} could be a highly symmetric site with inversion symmetry for the ordering distribution of Nb/W on the B sites (see Fig. S2 in the Supplemental Material [24]). For a truly random distribution of Nb/W atoms, however, the local symmetry of Eu^{3+} is lowered, so that the electric-dipole $^5D_0$-$^7F_2$ transition as well as the

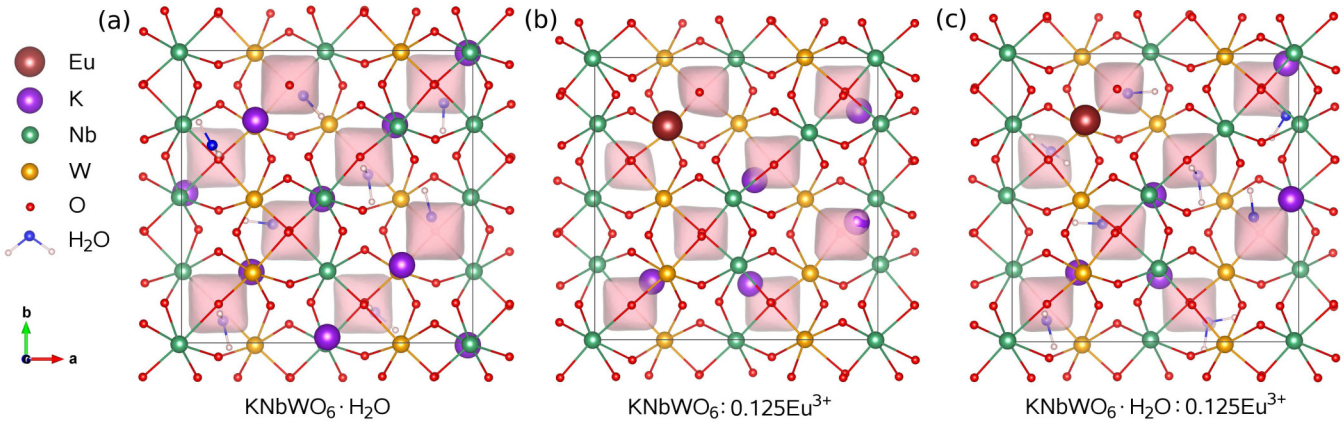

FIG. 2. Ball-and-stick view of unit cells with the lowest total energy for (a) the hydrated defect pyrochlore oxide $KNbWO_6 \cdot H_2O$, (b) the Eu-doped pyrochlore oxide $KNbWO_6$:$0.125Eu^{3+}$, and (c) the hydrated Eu-doped pyrochlore oxide $KNbWO_6 \cdot H_2O$:$0.125Eu^{3+}$, optimized by using the PBEsol+U method. The tetrahedronlike polyhedron with a light pink color indicates the BVS isosurface at a value of BVS = 1 for the K atom.

magnetic-dipole $^5D_0$-$^7F_1$ transition can be observed [13]. In addition, the random location of the surrounding K^+ ions inside the hollow spaces, due to their fractional occupancy of 1/4, can also lower the site symmetry of the Eu^{3+} ion. In this context, one can see that due to the existence of water molecules in the hollow spaces, the distribution of K^+ ions in the HydDop model is more symmetric than in the Dop model. Therefore, the hypersensitive electric-dipole $^5D_0$-$^7F_2$ transition is more likely in the dehydrated Dop model, in qualitative agreement with the experimental observation [13].

B. Electronic structure

Using the optimized models, i.e., Orig, Hyd, Dop, and HydDop models, with the lowest total energies, we calculated their electronic structures by means of the PBEsol+U method to investigate the luminescent properties. First, those of the undoped Orig and Hyd models are discussed. In these models, the band structures for spin-up and spin-down states were found to be identical to each other, and thus those for spin-up states were only shown in Figs. 3(a) and 3(b). The band gaps were calculated to be 3.00 eV for the defect pyrochlore oxide $KNbWO_6$ (Orig) and 3.03 eV for the hydrated $KNbWO_6 \cdot H_2O$ (Hyd), which can be said to be in reasonable agreement with the experimental value of 3.50 eV [36] compared with other GGA calculations for semiconductors, indicating the suitability of our selected U values. The almost identical band gap of the hydrated pyrochlore oxide with the original dehydrated one indicates that the water molecules inside the crystal hardly affect the electronic structure of the host material. Figures 3(c) and 3(d) display the density of states (DOS) for the spin-up states, projected on atomic orbitals. In both cases of Orig and Hyd models, the valence bands (VBs) were found to be dominantly originating from the O $2p$ states, while the conduction bands (CBs) were found to be composed of the $4d/5d$ states of Nb/W atoms and the O $2p$ states. For the case of the Hyd model, the electronic states of O and H atoms of the water molecule appeared in VBs, which are localized compared with the O $2p$ states of host. None of the states of the water molecule were observed in CBs, again indicating the relatively weak interaction between the water molecules and the host material.

Next, the electronic structure of the Eu-doped defect pyrochlore oxide $KNbWO_6$:$0.125Eu^{3+}$ (Dop model) is shown in Fig. 4. Due to different characteristics, we show the energy band structures and DOS for both the spin-up and spin-down states. As shown in Fig. 4(a), the band gap was estimated to be the same for the Orig model as 3 eV [Fig. 3(a)], and an unoccupied band was found above the valence band maximum (VBM), denoted by the dotted line. To clarify which atom contributes to this unoccupied band, the square of the band-decomposed wave function at the Γ point of the Brillouin zone (BZ) was plotted in Fig. 4(b). The isosurface of the wave-function square was found mostly around the Eu atom and partially around the nearby O atoms [Fig. 4(c)], indicating that this band is attributed to the Eu atom. In the orbital-resolved partial DOS (PDOS) plotted in Fig. 4(d), some of spin-up Eu $4f$ states can be found at a position of ∼3 eV below VBM, corresponding to the six occupied $4f$ orbitals, and one spin-up Eu $4f$ state is seen above VBM, just being responsible for the unoccupied $4f$ orbital of the Eu^{3+} ion. In the CB region, the spin-down $4f$ states and $5d$ states of Eu were found above CBM. It should be noted that except for Eu states, the other elements of the host material have almost the same characteristics of the Orig model: VB mostly comes from the O $2p$ states and CB is composed of the $4d/5d$ states of Nb/W atoms.

Figure 5 displays the electronic structure of the hydrated Eu-doped pyrochlore oxide $KNbWO_6 \cdot H_2O$:$0.125Eu^{3+}$ (HydDop model), calculated with the PBEsol+U method. As shown in Fig. 5(a) for its energy band structure, the band gap was calculated to be 2.73 eV, which is 0.30 eV lower than the value of the undoped Hyd model [see Fig. 3(b)], due to an upshift of VBM attributed to two spin-down bands. As in the Dop model, one unoccupied spin-up band was found over VBM, corresponding to the unoccupied Eu $4f$ state, as shown in Fig. 5(b) for the isosurface of the band-decomposed wave-function square at the Γ point. Meanwhile, the two occupied spin-down bands were revealed to originate from the oxygen atoms of the water molecules, as demonstrated

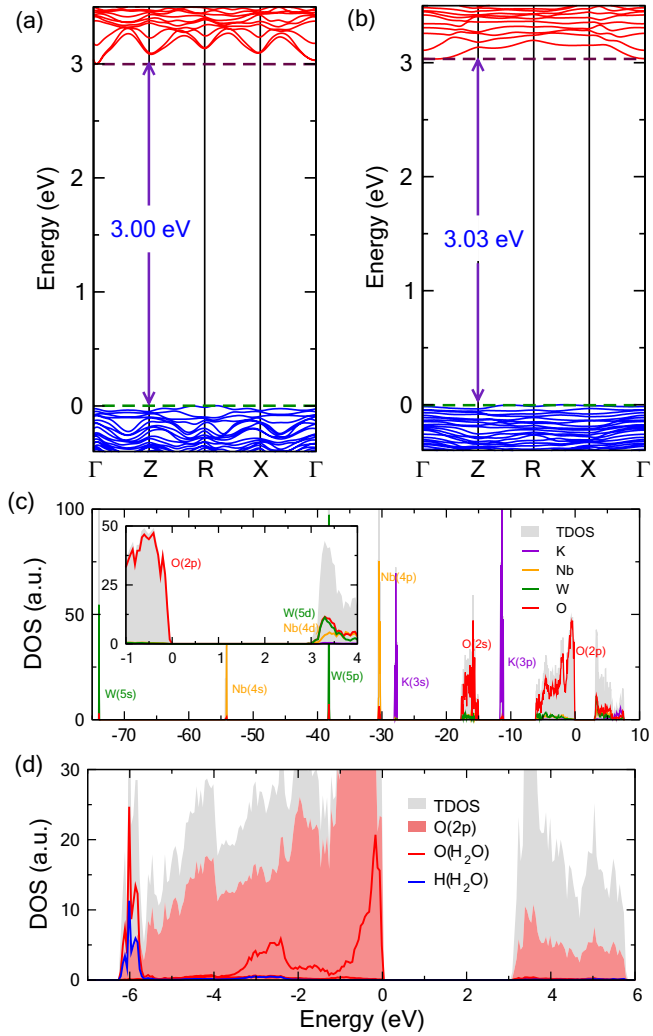

FIG. 3. Electronic band structure for (a) the defect pyrochlore oxide $KNbWO_6$ (Orig model) and (b) the hydrated defect pyrochlore oxide $KNbWO_6 \cdot H_2O$ (Hyd model). Density of states (DOS) for (c) the Orig model in the full energy range from −75 to 10 eV, where the inset shows the DOS around the Fermi level in detail, and (d) the Hyd model in the energy range from −7 to 6 eV, calculated by using the PBEsol+U method.

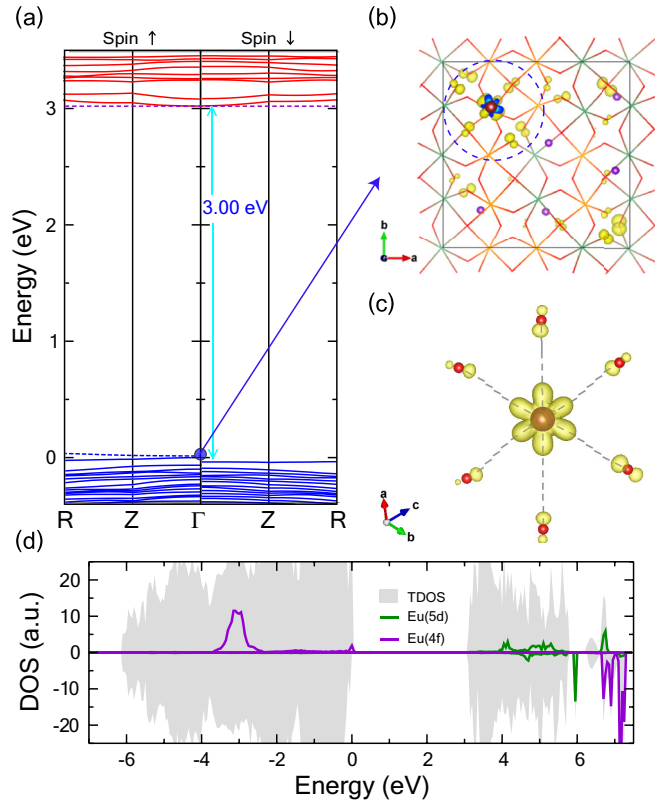

FIG. 4. Electronic structure of the Eu-doped defect pyrochlore oxide $KNbWO_6$:0.125Eu^{3+} (Dop model), calculated with the PBEsol+U method. (a) Energy band structure for spin-up and spin-down states with the dotted line for the unoccupied band and unchanged band gap of 3.00 eV, (b) isosurface view of the wave-function square at the Γ point, corresponding to the unoccupied Eu $4f$ state, and (c) its magnified view indicated by a dotted circle in (b), and (d) atomic orbital-resolved partial DOS.

in Fig. 5(c). It is worth noting that such an uplift of spin-down bands is not observed in the Hyd model, indicating that this is caused by an interaction between the doped Eu^{3+} ions and the water molecules. Such an interaction effect is more noticeable in the atomic orbital-resolved PDOS analysis shown in Fig. 5(d). When compared with the dehydrated Eu-doped Dop model [Fig. 3(a)], the spin-up Eu $4f$ states are found to be also divided into occupied and unoccupied parts, but the unoccupied state is observed to be clearly up-shifted from the valence band of the host material. In addition, the location of the spin-down Eu $4f$ states relative to the spin-up ones is more or less the same as the Dop model, but all the Eu $5d$ states move higher on the energy scale. When compared with the Hyd model [Fig. 3(b)], the occupied O $2p$ states of the water molecules in the HydDop model are clearly shown to be up-lifted over and rather dispersed on the valence band of the host material, indicating the enhanced interaction between water molecules and the host. Therefore, the water molecules in the HydDop model can be said to interact with both the doped Eu ion and the host, resulting in the formation of a so-called "bridge" that can mediate the nonradiative energy transfer from the activator Eu^{3+} ion to the host. Such a nonradiative energy transfer mediated by a water molecule might be a possible reason for the luminescence quenching effect observed in our previous experimental work [13].

C. Effect of oxygen vacancy on luminescence

In general, point defects play a critical role in luminescence since they can act as traps for photogenerated electrons, leading to a nonradiative recombination [21,37]. Considering that the oxygen vacancy V_O is the dominant point defect with the lowest formation energy in oxides, we investigated only the effect of oxygen vacancy on luminescence. Simulating oxygen vacancies with different charge states V_O^q is not a problem for the Orig and Hyd models: removing one oxygen atom and giving the charge q to the O-removed model. For the cases of the Eu-doped models (i.e., Dop and HydDop), however, the conferred charge on the model could be captured by the Eu^{3+} ion (becoming a Eu^{2+} ion) rather than by the oxygen vacancy

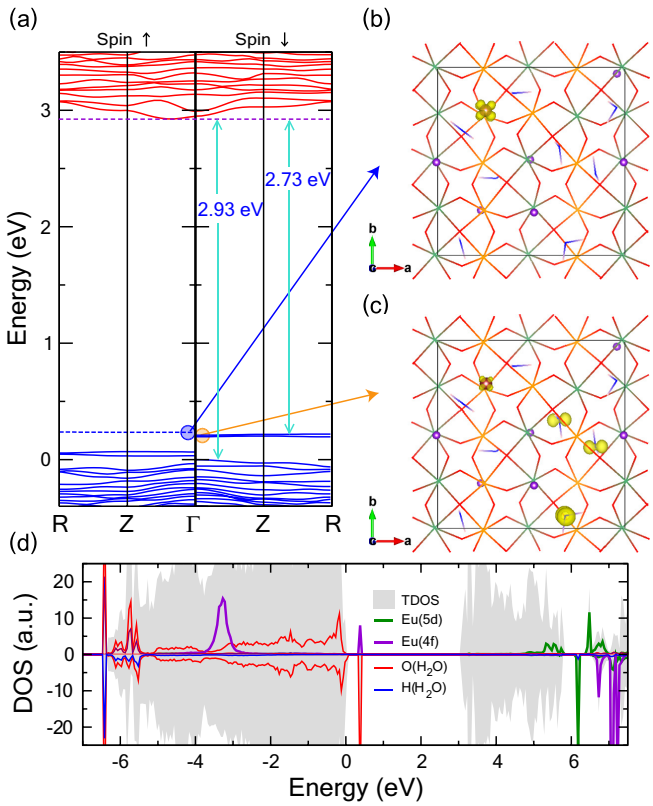

FIG. 5. Electronic structure of the hydrated Eu-doped defect pyrochlore oxide $KNbWO_6 \cdot H_2O{:}0.125Eu^{3+}$ (HydDop model), calculated with the PBEsol+U method. (a) Energy band structure for spin-up and spin-down sates, isosurface view of the wave-function square at the Γ point for (b) the unoccupied Eu $4f$ spin-up state and (c) occupied O $2p$ spin-down state of the water molecule, and (d) atomic orbital-resolved partial DOS.

V_O. To verify the charge state of the Eu ion in the existence of V_O, we calculated the band structures of the $KNbWO_6{:}Eu^{2+}$ model and Dop + V_O models with different total charges of −1, 0, +1, and +2 (see Fig. S3 in the Supplemental Material [24]). It turned out that the band structures of the Dop + V_O models with total charges of −1, 0 and +1 have a characteristic feature of $KNbWO_6{:}Eu^{2+}$—extremely localized flat bands from the seven Eu $4f$ spin-up states in the middle of the band gap region—whereas the Dop + V_O model with a total charge of +2 resembles that of $KNbWO_6{:}Eu^{3+}$. Therefore, the Dop + V_O models with total charges of −1, 0, +1, and +2 represent the defect states of Eu^{2+}/V_O^0, Eu^{2+}/V_O^{+1}, Eu^{2+}/V_O^{+2}, and Eu^{3+}/V_O^{+2}, respectively.

We estimated the formation energies of these oxygen vacancies using the following equation [37,38],

$$E_f\left(V_O^q\right) = E\left(\text{perf} + V_O^q\right) - E(\text{perf}) + \mu_O + q\varepsilon_F + E_{MP}, \quad (1)$$

where $E(\text{perf} + V_O^q)$ and $E(\text{perf})$ are the total energies of compounds with and without V_O^q, μ_O the chemical potential of oxygen, ε_F the Fermi energy, and E_{MP} the Makov-Payne correction term for the finite-size effect of charged model [39], as successfully applied in our previous works [40,41]. Here, μ_O was estimated to be half the total energy of the isolated oxygen molecule, and ε_F could be defined referencing the VBM of the host as $\varepsilon_F = \varepsilon_{VBM} + \Delta\varepsilon_F$, where $\Delta\varepsilon_F$ is varying between 0 and the band gap E_g. Similarly, the formation energies of the defects $Eu^{q_1}/V_O^{q_2}$ ($q_1 = +2$, +3 and $q_2 = 0$, +1, +2) can be calculated as follows,

$$E_f\left(Eu^{q_1}/V_O^{q_2}\right) = E\left(Eu^{q_1}/V_O^{q_2}\right) - E(Eu^{3+}) + \mu_O + (q_1 + q_2 - 3)\varepsilon_F + E_{MP}, \quad (2)$$

with reference to the total energies of the Dop or HydDop models without V_O, $E(Eu^{3+})$. Table III lists the calculated formation energies by using VBM as ε_F. It was revealed that in each case of different models, V_O^{+2} had the lowest formation energy, indicating that it is the oxygen vacancy with the highest possibility in the $KNbWO_6$-derived compounds, regardless of being hydrated or Eu doped. It should be highlighted that Eu^{3+}/V_O^{+2} has a remarkably higher formation energy compared to that of Eu^{2+}/V_O^{+2}, indicating that with oxygen vacancy the charge state of Eu^{3+} is readily reduced to Eu^{2+} with a half-filled electron configuration. The above discussion shows that O vacancies in this compound may act as a donor to reduce Eu^{3+} to Eu^{2+}. In fact, a similar mechanism by the Ba vacancy defect (V_{Ba}), acting as a donor, was proposed to explain the reduction of Eu^{3+} to Eu^{2+} observed in $BaAl_2O_4$:Eu phosphor prepared under a thermal carbon-reducing condition [42]. Once the Eu^{3+} is reduced to Eu^{2+}, it would exhibit characteristic broad emission spectra at around 500 nm due to the $4f$-$5d$ transition, in contrast to the sharp

TABLE III. Formation energies of oxygen vacancies with different charge states (V_O^q) and transition energies between the charge states.

	Orig	Hyd		Dop	HydDop
		Formation energy (eV)			
V_O^0	5.30	5.62	Eu^{2+}/V_O^0	5.36	5.54
V_O^{+1}	3.02	3.32	Eu^{2+}/V_O^{+1}	2.50	2.67
V_O^{+2}	1.28	1.76	Eu^{2+}/V_O^{+2}	0.01	0.28
			Eu^{3+}/V_O^{+2}	1.35	1.53
		Charge state transition energy (eV)			
$\varepsilon(2+/1+)$	1.74	1.56	$\varepsilon(2+/1+)(Eu^{2+})$	2.49	2.39
$\varepsilon(2+/0)$	2.00	1.93	$\varepsilon(2+/0)(Eu^{2+}$)	2.68	2.63
$\varepsilon(1+/0)$	2.27	2.29	$\varepsilon(1+/0)(Eu^{2+})$	2.86	2.87

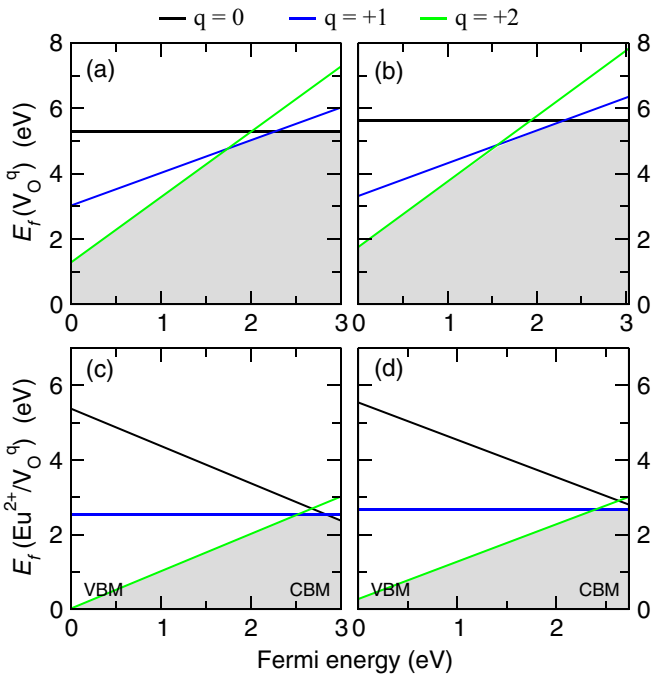

FIG. 6. Formation energies of oxygen vacancy with various charge states of $q = 0$, $+1$, and $+2$ in (a) the defect pyrochlore oxide $KNbWO_6$ (Orig) and (b) the hydrated one, $KNbWO_6 \cdot H_2O$ (Hyd), and of defects Eu^{2+}/V_O^q ($q = 0, +1, +2$) in (c) the Eu-doped one, $KNbWO_6$:0.125Eu^{3+} (Dop) and (d) the hydrated Eu-doped one, $KNbWO_6 \cdot H_2O$:0.125Eu^{3+} (HydDop), as a function of Fermi energy.

peaks in the emission spectra of Eu^{3+}. However, in our previous experiment, the absorption and emission spectra were found to have originated from the intraconfigurational $4f$-$4f$ transitions of Eu^{3+}, and no characteristics of $4f$-$5d$ transitions of Eu^{2+} were found [13]. Thus, once the doped Eu^{3+} ion is reduced to Eu^{2+}, it can no longer act as the luminescence center in this material, indicating that the oxygen vacancies are detrimental to luminescence. It is worth noting that all the $E_f(V_O^q)$ values in the hydrated compounds are higher than in the case of dehydrated ones, indicating that water molecules inside the host structural framework suppress the formation of oxygen vacancies.

For the charged oxygen vacancies, their formation energies vary with a change in the chemical potential of the electron reservoir ε_F in Eq. (1). Figure 6 presents the formation energies of oxygen vacancies in the models as a function of Fermi energy. The charge state of the oxygen vacancy with the lowest formation energy was found to change as the Fermi energy increases. When $E_f(V_O^q) = E_f(V_O^{q'})$ at a certain energy level, the charge state of V_O may change from V_O^q to $V_O^{q'}$ or vice versa by trapping or releasing the activated electron, and this energy level is defined as the charge state transition energy $\varepsilon(q/q')$. In the bottom part of Table III, the transition energies estimated by inspecting Fig. 6 were listed. It was clearly revealed that the transition energies in the Eu-doped models were found at a higher Fermi energy close to the CBM, whereas they were located in the middle of the band gap region. Importantly, $\varepsilon(2+/0)$ were estimated to be 2.68 and 2.63 eV in the Dop and Hyddop models, which are close to the transition energy 2.67 eV of $^7F_0 \rightarrow {}^5D_2$ being responsible for the major peak of 464 nm in the absorption spectra [13]. This indicates that the oxygen vacancy in the Dop and HydDop models can act as a trap for electrons excited by an incident radiation of 464 nm.

TABLE IV. Lattice constants (a, b, c), unit cell volume, and doping energy of $KNbWO_6$:0.125Ln^{3+} (Ln = Ce, Pr, Nd, Pm, Sm, Eu), calculated by using the PBEsol+U method.

Dopant	Lattice constants (Å)			Volume (Å^3)	E_{dop} (eV)
	a	b	c		
Ce	10.39	10.34	10.38	1115.82	0.10
Pr	10.39	10.34	10.38	1114.60	0.13
Nd	10.39	10.33	10.37	1113.72	0.19
Pm	10.39	10.33	10.37	1112.83	0.28
Sm	10.38	10.33	10.37	1112.04	0.39
Eu	10.38	10.33	10.36	1111.31	0.48

D. Ln^{3+} doping into $KNbWO_6$ (Ln = Ce, Pr, Nd, Pm, Sm)

Finally, we investigated the crystalline and electronic structures of other trivalent Ln ion-doped pyrochlore oxides $KNbWO_6$:0.125Ln^{3+} (Ln = Ce, Pr, Nd, Pm, Sm) with a calculation of the doping energy. As mentioned above, when the Ln^{3+} ion is doped into the pyrochlore oxide host $KNbWO_6$, three K^+ cations should be removed from the host to satisfy the charge neutrality. Then, the doping process can be thought to occur through (1) taking away three K atoms from the Orig model, leading to the formation of an intermediate phase, and (2) inserting one Ln atom into the intermediate phase to reach the Ln-doped compounds. For instance, the binding energies between the intermediate phase and three K atoms and one Eu atom can be calculated as follows,

$$E_b(3\text{K}) = E(\text{int}) + 3E(\text{K}) - E(\text{Orig}), \tag{3}$$

$$E_b(\text{Eu}) = E(\text{int}) + E(\text{Eu}) - E(\text{Dop}), \tag{4}$$

where E(int), E(Orig), and E(Dop) are the total energies of the crystalline compounds in the intermediate phase, the Orig and Dop model, and E(K) and E(Eu) are the total energies of isolated K and Eu atoms, respectively. Then the doping energy can be calculated as follows,

$$\begin{aligned} E_{\text{dop}} &= E(\text{Dop}) - E(\text{Eu}) + 3E(\text{K}) - E(\text{Orig}) \\ &= E_b(3\text{ K}) - E_b(\text{Eu}). \end{aligned} \tag{5}$$

Likewise, the doping energy in the case of the hydrated compound can be estimated from the total energies of the Hyd model E(Hyd) and HydDop model E(HydDop).

Table IV presents the optimized lattice constants and unit cell volumes of the Ln-doped pyrochlore oxides $KNbWO_6$:0.125Ln^{3+} (Ln = Ce, Pr, Nd, Pm, Sm, Eu) and their doping energies. As increasing the atomic number of the Ln dopant ion, the lattice constants and thus the unit cell volume were found to gradually decrease, for a unit cell volume from 1115.82 Å^3 for the Ce-doped to 1111.04 Å^3 for the Eu-doped compounds. Such a gradual decrease in the unit cell volume can be attributed to a decrease of the ionic radius of the Ln^{3+} ion as increasing the atomic number. The

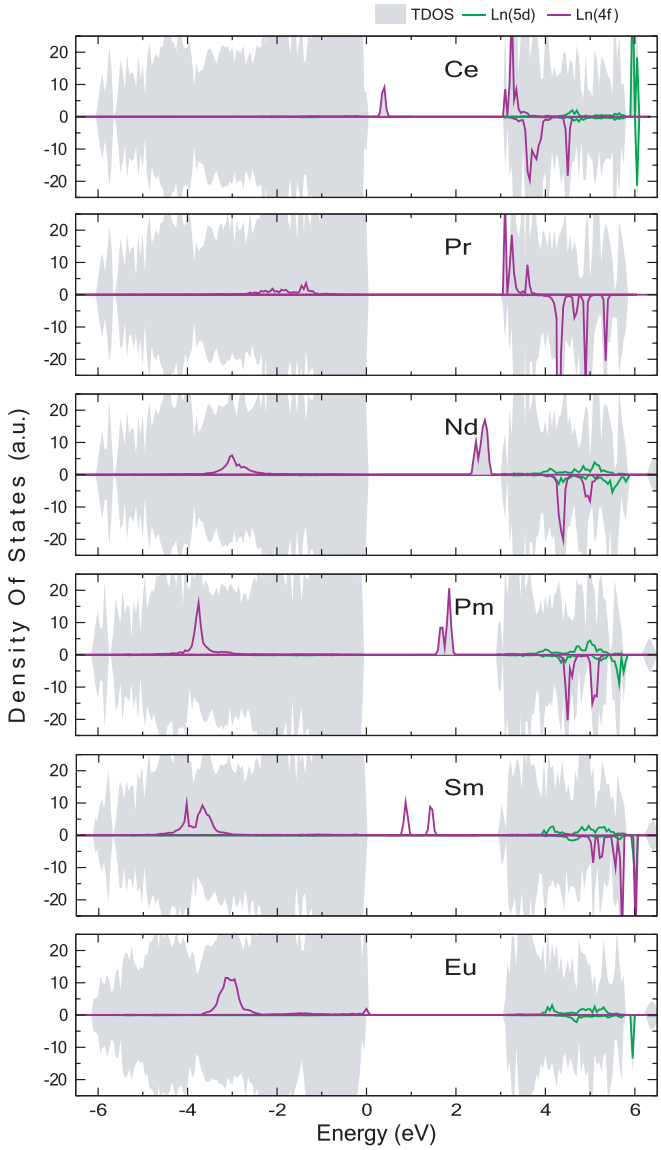

FIG. 7. Partial density of states in Ln-doped pyrochlore oxides $KNbWO_6$:0.125Ln^{3+} (Ln = Ce, Pr, Nd, Pm, Sm, Eu), calculated by using the PBEsol+U method.

doping energy was also found to systematically change; it increases from 0.10 eV for Ce doping to 0.48 eV for Eu doping. This indicates that doping Ln into $KNbWO_6$ is getting more difficult going from Ce to Eu. Conversely, $KNbWO_6$ can be said to serve as a better host material for Ce^{3+} doping than for Eu^{3+}. For the case of Eu doping into the Hyd model, the doping energy was calculated to be 0.57 eV, which is higher than into the Orig model (0.48 eV), indicating that the doping is more favorable in the dehydrated compound.

Figure 7 shows the atomic orbital-resolved PDOS in the Ln-doped pyrochlore oxides, highlighting the PDOS of Ln $5d$ and $4f$ states in the gray background of the total DOS. In all the Ln-doped compounds, the band gap identified by the tunneling density of states (TDOS) was found to barely change for different Ln ions but to be fixed at ∼3 eV. Commonly, the Ln^{3+} ions contain seven $4f$ orbitals, which are divided into occupied and unoccupied states. The number of occupied states corresponding to the spin-up electrons increases from 1 for Ce^{3+} to 6 for Eu^{3+}, while the unoccupied orbitals are for mostly spin-down states and some spin-up states. In the case of the Ce^{3+}-doped compound, the occupied spin-up state was found over the VBM, but in other cases they were located below the VBM. On the other hand, the unoccupied states were found above the CBM in the cases of Ce^{3+}- and Pr^{3+}-doped compounds, whereas they were found to gradually move towards the VBM going from Nd^{3+} through Pm^{3+} to Sm^{3+}. Even the unoccupied spin-up $4f$ state of Eu is located just above the VBM, as discussed above. It should be noted that as increasing the atomic number of the Ln ion, all the spin-up $4f$ states move downward, while the unoccupied spin-down $4f$ states move upward. Such a tendency of the $4f$ state positioning was observed by a first-principles study on a series of Ln^{3+}-doped $LaSi_3N_5$ (Ln = Ce, Pr, Nd, Pm, Sm, Eu) luminescent materials [43]. These imply that the defect pyrochlore oxides $KNbWO_6$ doped with Ln^{3+} can also exhibit a luminescent property, and therefore further experimental studies are required to verify their potentialities as luminescent materials.

IV. CONCLUSIONS

In this paper, we have carried out first-principles calculations to clarify several factors affecting the luminescence properties of defect pyrochlore oxide $KNbWO_6$-based materials. Several unit cell models have been suggested for crystalline $KNbWO_6$, its hydrated phase $KNbWO_6 \cdot H_2O$, Eu-doped phase $KNbWO_6$:0.125Eu^{3+}, and hydrated Eu-doped phase $KNbWO_6 \cdot H_2O$:0.125Eu^{3+}, in consideration of the random distribution of Nb/W atoms, water molecules, and Eu positions. Structural optimizations revealed that the local symmetry of the Eu^{3+} ion can be lowered in the dehydrated phase, giving an explanation for the experimental result of a ten times weaker emission at 612 nm owing to the electric-dipole $^5D_0$-$^7F_2$ by annealing. Through electronic structure calculations, the band gap of the host has been found to be almost the same as ∼3 eV in all the $KNbWO_6$-derived compounds. From the calculated DOS of $KNbWO_6$:0.125Eu^{3+}, the occupied spin-up $4f$ states of the Eu^{3+} ion were found below the VBM of the host, while the unoccupied spin-up state was found above the VBM. The observed up-shift of the unoccupied spin-up state from the VBM in $KNbWO_6 \cdot H_2O$:0.125Eu^{3+} indicates that water molecules could interact with the host and Eu^{3+} ion, mediating the nonradiative energy transfer between them and causing a quenching effect. When introducing the oxygen vacancy, the Eu^{3+} ion was found to be readily reduced to Eu^{2+}, leading to a detriment to the luminescence property, and, moreover, V_O was found to act as traps for the electrons activated by an incident light of 464 nm. Finally, the crystalline and electronic structures of $KNbWO_6$ doped with other Ln ions (Ln = Ce, Pr, Nd, Pm, Sm) have been investigated, concluding that $KNbWO_6$ can also be used as a luminescent host for doping a series of Ln^{3+} ions.

ACKNOWLEDGMENTS

This work is supported as part of the basic research project "Design of Innovative Functional Materials for Energy and Environmental Application" (No. 2016-20) by the State

Committee of Science and Technology, DPR Korea. Computation was done on the HP Blade System C7000 (HP BL460c) that is owned by Faculty of Materials Science, Kim Il Sung University.

[1] J. Fang, M. Saunders, Y. Guo, G. Lu, C. L. Raston, and K. S. Iyer, Chem. Commun. **46**, 3074 (2010).
[2] W. Yang, X. Li, D. Chi, H. Zhang, and X. Liu, Nanotechnology **25**, 482001 (2014).
[3] X. Huang, S. Han, W. Huang, and X. Liu, Chem. Soc. Rev. **42**, 173 (2013).
[4] F. Chi, X. Wei, B. Jiang, Y. Chen, C. Duan, and M. Yin, Dalton Trans. **47**, 1303 (2018).
[5] F. Chen, M. Chen, C. Yang, J. Liu, N. Luo, G. Yang, D. Chen, and L. Li, Phys. Chem. Chem. Phys. **17**, 1189 (2015).
[6] B. Mutlet, S. Boudin, O. Perez, J. M. Rueff, C. Labbe, and P. A. Jaffres, Dalton Trans. **44**, 1186 (2015).
[7] L. Lovisa, J. Andres, L. Gracia, M. Li, C. Paskocimas, M. Bomio, V. Araujo, E. Longo, and F. Motta, J. Alloys Compd. **695**, 3094 (2017).
[8] Y. Jia, A. Miglio, S. Ponce, M. Mikami, and X. Gonze, Phys. Rev. B **96**, 125132 (2017).
[9] J. Zhong, W. Zhao, L. Yang, P. Shi, Z. Liao, M. Xia, W. Pu, W. Xiao, and L. Wang, RSC Adv. **8**, 13054 (2018).
[10] X. Li, H. Cai, L. Ding, X. Dou, and W. Zhang, J. Alloys Compd. **541**, 36 (2012).
[11] S. Fujihara and K. Tokumo, Chem. Mater. **17**, 5587 (2005).
[12] M. M. Gentleman and D. R. Clarke, Surf. Coat. Technol. **200**, 1264 (2005).
[13] Y. N. Han, S. Jiao, M. Xu, Y. Xu, G. Pang, and S. Feng, RSC Adv. **4**, 24142 (2014).
[14] Y. N. Han, S. Jiao, M. Xu, G. Pang, and S. Feng, RSC Adv. **4**, 14357 (2014).
[15] B. Gr˘eta, D. Lützenkrichen-Hecht, M. Vrankić, S. Bosnar, A. Šarić, M. Takahashi, D. Petrov, and M. Bišćan, Inorg. Chem. **57**, 1744 (2018).
[16] Y. Jia, S. Ponce, A. Miglio, M. Mikami, and X. Gonze, Adv. Opt. Mater. **5**, 1600997 (2017).
[17] H. Daicho, Y. Shinomiya, K. Enomoto, A. Nakano, H. Sawa, S. Matsuishi, and H. Hosono, Chem. Commun. **54**, 884 (2017).
[18] S. Ponce, Y. Jia, M. Giantomassi, M. Mikami, and X. Gonze, J. Phys. Chem. C **120**, 4040 (2015).
[19] M.-H. Du, ECS J. Solid State Sci. Technol. **5**, R3007 (2016).
[20] B. Qu, B. Zhang, L. Wang, R. Zhou, and X. C. Zeng, Chem. Mater. **27**, 2195 (2015).
[21] Y. Jia, A. Miglio, M. Mikami, and X. Gonze, Phys. Rev. Materials **2**, 125202 (2018).
[22] S. Adams, Acta Cryst. B **57**, 278 (2001).
[23] L. L. Wong, H. Chen, and S. Adams, Phys. Chem. Chem. Phys. **19**, 7506 (2017).
[24] See Supplemental Material at http://link.aps.org/supplemental/10.1103/PhysRevB.102.035131 for crystalline structures of the experimentally identified defect pyrochlore $KNbWO_6$ and $KNbWO_6 \cdot H_2O$ along with an isosurface plot of the bond valence sum in these compounds, a table for the structural properties of several hydrated and Eu-doped compounds, a polyhedral view of the local symmetry of a doped Eu^{3+} ion, and band structure graphs of $KNbWO_6 \cdot H_2O$:Eu+V_O with different total charges of $q = -1, 0, 1, 2$.
[25] P. W. Barnes, P. M. Woodward, Y. Lee, T. Vogt, and J. A. Hriljac, J. Am. Chem. Soc. **125**, 4572 (2003).
[26] P. Giannozzi, S. Baroni, N. Bonini, M. Calandra, R. Car *et al.*, J. Phys.: Condens. Matter **21**, 395502 (2009).
[27] K. F. Garrity, J. W. Bennet, K. M. Rabe, and D. Vanderbilt, Comput. Mater. Sci. **81**, 446 (2014).
[28] J. P. Perdew, K. Burke, and M. Ernzerhof, Phys. Rev. Lett. **77**, 3865 (1996).
[29] J. P. Perdew, A. Ruzsinszky, G. I. Csonka, O. A. Vydrov, G. E. Scuseria, L. A. Constantin, X. Zhou, and K. Burke, Phys. Rev. Lett. **100**, 136406 (2008).
[30] I. Timrov, N. Marzari, and M. Cococcioni, Phys. Rev. B **98**, 085127 (2018).
[31] H. J. Monkhorst and J. D. Pack, Phys. Rev. B **13**, 5188 (1976).
[32] A. Dal Corso, Comput. Mater. Sci. **95**, 337 (2014).
[33] D. W. Murphy, R. J. Cava, K. Rhyne, R. S. Roth, A. Santoro, S. M. Zahurak, and J. L. Dye, Solid State Ionics **18**, 799 (1986).
[34] S. K. Mahesh, P. P. Rao, M. Thomas, A. N. Radhakrishnan, and P. Koshy, J. Mater. Sci.: Mater. Electron. **23**, 1605 (2012).
[35] S. K. Mahesh, P. P. Rao, M. Thomas, T. L. Francis, and P. Koshy, Inorg. Chem. **52**, 13304 (2013).
[36] X. Zeng, Y. Chen, S. Jiao, Z. Fang, B. Wang, G. Pang, and S. Feng, New J. Chem. **42**, 5753 (2018).
[37] C. Freysoldt, B. Grabowski, T. Hickel, J. Neugebauer, G. Kresse, A. Janotti, and C. G. Van de Walle, Rev. Mod. Phys. **86**, 253 (2014).
[38] C. G. Van de Walle and J. Neugebauer, J. Appl. Phys. **95**, 3851 (2004).
[39] G. Makov and M. C. Payne, Phys. Rev. B **51**, 4014 (1995).
[40] Y.-H. Kye, C.-J. Yu, U.-G. Jong, Y. Chen, and A. Walsh, J. Phys. Chem. Lett. **9**, 2196 (2018).
[41] Y.-H. Kye, C.-J. Yu, U.-G. Jong, C.-N. Sin, and W. Qin, J. Mater. Chem. C **7**, 15148 (2019).
[42] M. Peng and G. Hong, J. Lumin. **127**, 735 (2007).
[43] I. A. M. Ibrahim, Z. Lences, P. Sajgalik, L. Benco, and M. Marsman, J. Lumin. **164**, 131 (2015).